A Dual-Mode Model Predictive Control Algorithm Trajectory Tracking in Discrete-Time Nonlinear Dynamic Systems

Asad A. Ul Haq[1]
Department of Mechanical Engineering,
The University of Texas at Austin,
Austin, TX 78705
e-mail: asadulhaq@utexas.edu

Michael E. Cholette
Science and Engineering Faculty,
Queensland University of Technology,
Brisbane, QLD 4001, Australia
e-mail: michael.cholette@qut.edu.au

Dragan Djurdjanovic
Department of Mechanical Engineering,
The University of Texas at Austin,
Austin, TX 78705
e-mail: dragand@me.utexas.edu

In this paper, a dual-mode model predictive/linear control method is presented, which extends the concept of dual-mode model predictive control (MPC) to trajectory tracking control of nonlinear dynamic systems described by discrete-time state-space models. The dual-mode controller comprises of a time-varying linear control law, implemented when the states lie within a sufficiently small neighborhood of the reference trajectory, and a model predictive control strategy driving the system toward that neighborhood. The boundary of this neighborhood is characterized so as to ensure stability of the closed-loop system and terminate the optimization procedure in a finite number of iterations, without jeopardizing the stability of the closed-loop system. The developed controller is applied to the central air handling unit (AHU) of a two-zone variable air volume (VAV) heating, ventilation, and air conditioning (HVAC) system. [DOI: 10.1115/1.4035096]

1 Introduction

Since it first gained popularity in the 1970s, MPC of linear systems has reached an advanced level of maturity in both theory and practice [1]. The past two decades have seen growing interest in the theory and implementation of MPC of nonlinear systems [2], with applications spreading from the roots of MPC in the process industry [3] into other areas, including aerospace and automotive fields [4].

The basic notion in MPC is to repeatedly solve a finite-horizon optimal control problem at every sample time and implement the first element of the obtained control sequence [3]. There are a number of significant advantages that result from MPC strategies, including straightforward formulation and implementation of control for constrained, time-varying, and nonlinear systems. There are a number of survey and review publications that look at MPC development in both academia and industry [1,4–6]. Other works in nonlinear MPC have looked at the implementation with both physics-based and data-driven models, e.g., with artificial neural networks (ANNs) [7], Takagi-Sugeno fuzzy models (TSFMs) [8], and NARMAX models [9] all of which result in nonlinear discrete-time models.

The concept of dual-mode MPC, proposed by Michalska and Mayne [10], has been considered in numerous works to overcome the requirement for optimality to prove suitability for classical MPC, especially where nonlinear dynamics and/or constraints exist. The papers by Chen and Allgöwer [11] and Scokaert et al. [12] consider the implications of suboptimal solutions of the MPC problem on the stability of the closed-loop system and utilize linear controllers in a neighborhood of the target state. While there are suboptimal MPC approaches that are not dual-mode in nature, the works mentioned previously [10–12] discuss the issues associated with these methods and motivate the preference of dual-mode methods, which are the focus of this work. Nguyen and Gutman [13] developed such a dual-mode MPC for linear time invariant (LTI) systems, while Al-Gherwi et al. [14] applied the dual-mode MPC concept for robust distributed control of time-varying linear systems. Açikmese and Carson [15] proposed a combined feedforward and feedback control strategy, with MPC providing the feedforward component and the feedback component being designed to independently ensure that the state remains within a ball centered around the origin.

Trajectory tracking using MPC has also been considered for linear time invariant (LTI) systems [16,17]. Limon et al. [18] looked at trajectory planning such that the trajectory converges to a periodic signal. Chisci et al. [19] considered MPC tracking for linear parameter varying (LPV) models. On the other hand, Magni et al. [20] considered MPC of nonlinear systems with a longer prediction horizon than the control horizon, with the intent to enlarge the terminal set. Kuhne et al. [21] considered nonlinear wheeled mobile robots (WMRs) and compared both linear and nonlinear MPC, though formal stability considerations are omitted.

The concept of dual-mode MPC methods for trajectory tracking tasks for continuous-time nonlinear systems is considered by Faulwasser and Findeisen [22]. They use time-varying terminal sets and a locally stabilizing linear control law to guarantee stability.

In this paper, we extend dual-mode MPC to trajectory tracking for a nonlinear dynamic systems described by discrete-time state-space models. Characterization of the terminal constraint in the MPC problem, which serves as the switching surface between the two controllers, is offered along with the proof of stability for the resulting algorithm. A simulated application is also presented here: control of the central AHU of a HVAC system modeled so as to include several nonlinearities that are typically omitted from MPC applications for supervisory control of HVAC systems.

The remainder of this paper is organized as follows: Section 2 contains the notation, model structure, and assumptions used in this work. In Sec. 3, a dual-mode model predictive linear controller (DMMPLC) strategy is detailed, and the stability of the closed-loop system is established. Section 4 contains results of the simulated implementation of the DMMPLC approach to the AHU of a VAV HVAC system. Conclusions and future work are discussed in Sec. 5.

2 Preliminaries

2.1 Notation. In the sequel, the following notation conventions will be adopted. All the sampling times will appear as subscripts, N shall be used to refer to the MPC horizon and T_{final} represents the end time of the entire control task. Bold faced symbols will represent sequences. For instance, $\boldsymbol{u}_k = \{u_{k|k}, u_{k+1|k}, \ldots, u_{k+N-1|k}\}$ will denote a control sequence starting at the current sampling time, k, and continuing up to $k+N-1$. Note that the corresponding state sequences will have an additional term at the end, $\boldsymbol{x}_k = \{x_k, x_{k+1}, \ldots, x_{k+N-1}, x_{k+N}\}$. Underlined bold faced symbols shall be used to denote sequences

[1]Corresponding author.

Contributed by the Dynamic Systems Division of ASME for publication in the Journal of Dynamic Systems, Measurement, and Control. Manuscript received March 31, 2016; final manuscript received October 21, 2016; published online February 9, 2017. Assoc. Editor: Zongxuan Sun.

that span the time of the entire control task. For example, $\underline{\boldsymbol{r}} = \{r_0, r_1, \ldots, r_{T_{\text{final}}}\}$ will denote the entire reference sequence that is to be tracked by the system outputs. An asterisk $(*)$ will be used to denote optimal quantities and for a matrix $A \in \mathbb{R}^{p\times p}$, $A > 0$ denotes positive definiteness.

2.2 Model Structure and Assumptions. The model structure shall be taken to be the standard nonlinear discrete-time state-space form

$$\begin{aligned} x_{k+1} &= f(k, x_k, u_k) \\ y_k &= h(x_k) \end{aligned} \tag{1}$$

where x_k is the state vector at sampling time k. The system dimensions are given by $x \in \mathbb{R}^n$, $u \in \mathbb{R}^m$, and $y \in \mathbb{R}^q$.

The discretization of a nonlinear continuous-time state-space model is a task that can be tackled using various approaches [23–25] or may arise directly from system identification procedures (e.g., NARMAX models). The assumptions are listed below:

(1) The system is assumed to allow at least two differentials with respect to both the input and state.
(2) The entire reference trajectory is assumed to be known ahead of time.
(3) It is assumed that a control sequence exists such that error-free tracking can be achieved.
(4) The reference trajectory is reachable, for some reasonable time horizon, at the initial sample time.
(5) Any disturbances are known ahead of time and can be eliminated from the system dynamics model.

When Assumption 4 does not hold true, the reference sequence is often replaced with a reachable target that is "close" to it [5]. Nevertheless, such trajectory planning problems will not be considered here.

The reference state sequence $\underline{\boldsymbol{x}}^r$ and reference control input sequence[2] $\underline{\boldsymbol{u}}^r$ that lead to perfect output tracking can then be used to define the tracking error as $\tilde{x}_k = x_k - x_k^r$, with its dynamics being described by

$$\tilde{x}_{k+1} = \tilde{f}(k, \tilde{x}_k, \tilde{u}_k) \tag{2}$$

where $\tilde{u}_k = u_k - u_k^r$ and $\tilde{f}(k, \tilde{x}_k, \tilde{u}_k) \triangleq f(k, x_k^r + \tilde{x}_k, u_k^r + \tilde{u}_k) - x_{k+1}^r$. An equivalent of the previous control goal is to then use the "virtual" control input $\tilde{u}$ to drive the tracking error to the origin.

3 Dual-Mode Model Predictive/Linear Control

3.1 Model Predictive Control Algorithm and Sequential Quadratic Programing. A finite-horizon nonlinear optimal control problem (NL-OCP) can be postulated in the error space as follows:

$$\begin{aligned} \underset{\tilde{\boldsymbol{u}}_k}{\text{minimize}} \quad & J_N(\tilde{\boldsymbol{x}}_k, \tilde{\boldsymbol{u}}_k) = \sum_{i=k}^{k+N-1} \ell(\tilde{x}_i, \tilde{u}_i) + V_f(\tilde{x}_{k+N}) \\ \text{subject to:} \quad & \tilde{x}_{k+1} = \tilde{f}(k, \tilde{x}_k, \tilde{u}_k) \\ & \tilde{x}_0 = x_0 - x_0^r \\ & \tilde{x}_{k+N} \in \tilde{\mathbb{X}}_f \\ & \tilde{u}_k \in \tilde{\mathcal{U}}_k \end{aligned} \tag{3}$$

where $\ell(\tilde{x}_i, \tilde{u}_i) = \tilde{x}_i^{\mathrm{T}} Q \tilde{x}_i + \tilde{u}_i^{\mathrm{T}} R \tilde{u}_i$ and $V_f(\tilde{x}_{k+N}) = \tilde{x}_{k+N}^{\mathrm{T}} Q_f \tilde{x}_{k+N}$, with R, Q, and Q_f being symmetric, positive definite matrices of appropriate dimensions and $\tilde{\mathbb{X}}_f$ being a neighborhood around the origin of the error space. $\tilde{\mathcal{U}}_k$ is defined based on the values of u_k^r and the set $\mathcal{U}$, which is the set of allowable control inputs to the system (1). NL-OCP (3) is solved at each sampling instant, and the first element of the control sequence obtained is implemented.

It is well known that a receding horizon control strategy does not necessarily guarantee stability of the closed-loop system [5]. A common formulation that leads to closed-loop stability is to use a point terminal state constraint [26], $\tilde{x}_{k+N} \in \{0\} = \tilde{\mathbb{X}}_f$. The stability of the resulting MPC algorithm is established per Theorem 5.2 of Ref. [27].

Recent research proposes the use of sequential quadratic programs (SQPs) employing sequential linearizations of the constraints in the NL-OCP in order to efficiently solve it [28]. However, this approach converges to a local optimum of the NL-OCP defined in Eq. (3), if and only if the system is locally N-step controllable [28]. Additionally, the terminal equality constraint is only satisfied as the number of SQP iterations tends to infinity, rendering the stability guarantees based on this constraint moot in practice.

3.2 Dual-Mode Model Predictive Control Design. The concept of dual-mode MPC [10] is extended here for tracking of time-varying reference trajectories for discrete-time nonlinear systems. The introduced controller, incorporating an MPC component and a time-varying linear control law, shall also overcome the need for an infinite number of iterations to meet a terminal equality constraint and reliance on global optimality to establish stability. The notion is to design a locally stabilizing control law and characterize a positively invariant set around the reference trajectory under that control law. The boundary of that set will be used as a terminal constraint set $\tilde{\mathbb{X}}_f$ to replace the equality constraint in Eq. (3). While the state is outside this set, a control sequence satisfying the constraints of the NL-OCP (3) can be pursued via an SQP procedure, and the locally stabilizing control law can be employed once the state enters this set.

In order to design a locally stabilizing controller and characterize the corresponding switching surface, the dynamics will be linearized about the reference trajectory. A time-varying linear controller of the form $\tilde{u}_k = K_k \tilde{x}_k$ will be pursued. The key is to characterize terminal constraint sets that are compact, convex, and positively invariant under the local controller and the actual *nonlinear* system dynamics. Terminal constraint sets shall be pursued in the form $\mathbb{W}_k = \{\tilde{x}_k | \tilde{x}_k^{\mathrm{T}} P_k \tilde{x}_k \le \varepsilon\}$, where P_k and ε will be determined so as to ensure the positive invariance of $\mathbb{W}_k$ under the time-varying linear control law.

3.2.1 Characterizing the Local Linear Control Law and Switching Surface. The actual error dynamics are

$$\tilde{x}_{k+1} = A_k^{cl} \tilde{x}_k + e(\tilde{x}_k) \tag{4}$$

where $e(\tilde{x}_k) = \tilde{f}(k, \tilde{x}_k, K_k \tilde{x}_k) - A_k^{cl} \tilde{x}_k$ is the linearization error and $A_k^{cl} = A_k + B_k K_k$. The time-varying linear control gain K_k can be obtained via an linear matrix inequality (LMI) as described in Lemma 1.

LEMMA 1. (Design of a locally stabilizing time-varying linear control law)

Consider the time-varying linear system

$$\tilde{x}_{k+1} = A_k \tilde{x}_k + B_k \tilde{u}_k \tag{5}$$

and let Q and R be the symmetric, positive definite matrices used in the definition of J_N. For $k = 0, 1, \ldots, T_{\text{final}} - 1$, let Γ_k and Φ_k satisfy

$$\begin{bmatrix} \Gamma_k & (A_k\Gamma_k + B_k\Phi_k)^{\mathrm{T}} & \mu^{\frac{1}{2}}\Gamma_k^{\mathrm{T}} Q^{\frac{1}{2}} & \mu^{\frac{1}{2}}\Phi_k^{\mathrm{T}} R^{\frac{1}{2}} \\ A_k\Gamma_k + B_k\Phi_k & \Gamma_{k+1} & 0 & 0 \\ \mu^{\frac{1}{2}} Q^{\frac{1}{2}}\Gamma_k & 0 & \mathrm{I} & 0 \\ \mu^{\frac{1}{2}} R^{\frac{1}{2}}\Phi_k & 0 & 0 & \mathrm{I} \end{bmatrix} \ge 0 \tag{6}$$

[2]Although $\underline{\boldsymbol{x}}^r$ and $\underline{\boldsymbol{u}}^r$ may be obtained by any approach, an auxiliary optimization problem to obtain these is provided in the Appendix.

with $\mu > 1$. *Then, the time-varying control gains* $K_k = \Phi_k \Gamma_k^{-1}$, $k = 0, 1, \ldots, T_{\text{final}} - 1$, *guarantee closed-loop stability of Eq. (5) for* $k \in \{0, 1, \ldots, T_{\text{final}}\}$. *These gains also guarantee that*

$$(A_k + B_k K_k)^{\mathrm{T}} P_{k+1} (A_k + B_k K_k) - P_k \leq -\mu \bar{Q}_k \tag{7}$$

with $\bar{Q}_k = Q + K_k^{\mathrm{T}} R K_k$.

Proof. The sketch of the proof is based on the conversion of Eq. (7) into an LMI via Schur complements and instituting the change of variables $\Gamma_k = P_k^{-1}$ and $\Phi_k = K_k \cdot P_k^{-1}$. □

Remark 1. The practical implementation of Lemma 1 is carried out in reverse order, from $k = T_{\text{final}}$ to $k = 1$. $P_{T_{\text{final}}}$ may be set to any symmetric positive definite matrix, e.g., $\mathbf{I}$.

Since the linear control law is designed based on linearized dynamics (5), the resulting stability can only be expected to hold within a sufficiently small neighborhood of the reference trajectory, where the linearization error remains sufficiently small. It is also known that the linearization error $e(\tilde{x}_k)$ satisfies $\lim_{||\tilde{x}_k|| \to 0} \frac{||e(\tilde{x}_k)||}{||\tilde{x}_k||} \to 0$ [29].

It is now possible to determine an upper bound on the linearization error $e(\tilde{x}_k)$ for which the linear control law guarantees closed-stability even when applied to the original *nonlinear* system dynamics (1).

LEMMA 2. (Cost reduction inside $\mathbb{W}_k$, under the linear control law))

Let the matrices P_k *and* $\bar{Q}_k$ *be defined as in Lemma 1 and consider a Lyapunov-like cost function* $V_k = \tilde{x}_k^{\mathrm{T}} P_k \tilde{x}_k$, *with* $\Delta V_k = V_{k+1} - V_k$. *Also, let* γ_k, $\forall k \in \{0, 1, \ldots, T_{\text{final}} - 1\}$ *satisfy*

$$\gamma_k \leq \frac{\left(-c_{2_k} + \sqrt{c_{2_k}^2 + (\mu - 1) c_{1_k} c_{3_k}}\right)}{c_{1_k}} \tag{8}$$

where $c_{1_k} \triangleq \lambda_{\max}(P_{k+1})$, $c_{2_k} \triangleq ||P_{k+1} A_k^{cl}||$ *and* $c_{3_k} \triangleq \lambda_{\min}(\bar{Q}_k)$, *with* μ *defined in Lemma 1 and* $\lambda_{\max}$ *and* $\lambda_{\min}$ *being the largest and smallest eigenvalues, respectively. Also, let* ε *be such that* $\mathbb{W}_k = \{\tilde{x}_k^{\mathrm{T}} P_k \tilde{x}_k \leq \varepsilon\}$

$$\tilde{x}_k \in \mathbb{W}_k \Rightarrow ||e(\tilde{x}_k)|| < \gamma_k ||\tilde{x}_k||$$

Then,

$$\Delta V_k < -\tilde{x}_k^{\mathrm{T}} \bar{Q}_k \tilde{x}_k, \forall\ \tilde{x}_k \in \mathbb{W}_k, \quad k \in \{0, 1, \ldots, T_{\text{final}} - 1\}$$

Proof. The proof of this lemma is established by manipulation of the Lyapunov inequality $(A_k^{cl} \tilde{x}_k + e(\tilde{x}_k))^{\mathrm{T}} P_{k+1} (A_k^{cl} \tilde{x}_k + e(\tilde{x}_k)) - \tilde{x}_k^{\mathrm{T}} P_k \tilde{x}_k < -\tilde{x}_k^{\mathrm{T}} \bar{Q}_k \tilde{x}_k$, which directly incorporates an upper bound on the linearization error. □

The following proposition completes the characterization of $\mathbb{W}_k$ by tackling the problem of determining ε.

PROPOSITION 1. (Determining the terminal constraint set $\mathbb{W}_k$)

Select $\varepsilon = \min_k(\lambda_{\min}(P_k) \varepsilon_{1_k}^2)$ *with* $\varepsilon_{1_k} = \min\left(\frac{\gamma_k}{c_{2_k}}, \delta\right)$, *where* γ_k *is defined as in Lemma 2,* $\delta\mathcal{B}$ *is some small hyperspherical neighborhood of the origin in the error space, and* c_k *is the solution of the following optimization problem:*

$$c_k = \max_{\tilde{x} \in \delta\mathcal{B}} \left(\frac{1}{2} \left\| \frac{\partial^2 \tilde{f}}{\partial \tilde{x}^2} \Big|_{\bar{x}, \bar{u}} + 2 \frac{\partial^2 \tilde{f}}{\partial \tilde{x} \partial \tilde{u}} \Big|_{\bar{x}, \bar{u}} K_k + K_k^{\mathrm{T}} \frac{\partial^2 \tilde{f}}{\partial \tilde{u}^2} \Big|_{\bar{x}, \bar{u}} K_k \right\| \right)$$

with $\tilde{u}_k = K_k \tilde{x}_k$. *The Lyapunov-like cost function,* $V_k = \tilde{x}_k^{\mathrm{T}} P_k \tilde{x}_k$, *is monotonically decreasing inside the resulting set* $\mathbb{W}_k = \{\tilde{x}_k^{\mathrm{T}} P_k \tilde{x}_k \leq \varepsilon\}$, *under the proposed linear control law. This renders the set* $\mathbb{W}_k$ *positively invariant*.

Proof. Due to space constraints only the general idea of the proof is sketched here. The proof utilizes the lagrange error bound (LEB) and the time-varying linear control $\tilde{u}_k = K_k \tilde{x}_k$. An upper bound c_k on the linearization error, within some ball $\delta\mathcal{B}$ around the origin, is established based on the LEB and the comparison with the allowable linearization error γ_k defines ε_{1_k}. □

The determination of c_k in the above proposition involves finding the maximum value of a nonlinear function within a neighborhood of the origin. This can be achieved by exploiting the approach described in Ref. [30], which converges to a local optimum. The local nature of this solution is sufficient for practical purposes.

LEMMA 3. (Positive invariance of the set sequence $\mathbb{W}_k$ under the linear control law).

Let P_k, K_k, *and* $\mathbb{W}_k$ *be defined as in Lemmas 1 and 2, respectively. For the system error dynamics given by Eq. (2), invoking Lemma 2 leads to* $\tilde{x}_k \in \mathbb{W}_k \Rightarrow \tilde{x}_{k+1} \in \mathbb{W}_{k+1}$ *under the linear control law* $\tilde{u}_k = K_k \tilde{x}_k$. *In other words, once* $\tilde{x}_k$ *enters* $\mathbb{W}_k$, *the cost reduction in Lemma 1 holds for the remaining time of the control task*.

Proof. The definitions of V_k and $\mathbb{W}_k$ from Lemma 2 give $\tilde{x}_k^{\mathrm{T}} P_k \tilde{x}_k \leq \varepsilon$, $\forall \tilde{x}_k \in \mathbb{W}_k$, and it has been established that, under the linear controller, $\forall \tilde{x}_k \in \mathbb{W}_k$, $\Delta V_k < 0$, which implies that $\tilde{x}_{k+1}^{\mathrm{T}} P_{k+1} \tilde{x}_{k+1} \leq \tilde{x}_k^{\mathrm{T}} P_k \tilde{x}_k \leq \varepsilon$, $\forall \tilde{x}_k \in \mathbb{W}_k$ and thus $\tilde{x}_k \in \mathbb{W}_k \Rightarrow \tilde{x}_{k+1} \in \mathbb{W}_{k+1}$. □

Note that the invariant region $\mathbb{W}_k$ estimated by the proposed method is not necessarily the largest possible set and maximizing its size may reduce the required SQP iterations. However, such maximization of the size of $\mathbb{W}_k$ is beyond the scope of this paper.

3.2.2 The Dual-Mode Model Predictive/Linear Control Algorithm. A dual-mode control algorithm with an MPC control horizon of N, in conjunction with the linear control law defined using Lemma 1, can be implemented in the form of Algorithm 1.

Algorithm 1 Dual-mode model predictive/linear control

1: **OFFLINE**
2: Select μ and compute K_k, P_k using Lemma 1
3: Compute γ_k using Lemma 2
4: Select δ and compute ε_{1_k} using Proposition 1
5: Set $\varepsilon = \min_k(\lambda_{\min}(P_k) \varepsilon_{1_k}^2)$ and $\mathbb{W}_k = \{\tilde{x}_k^{\mathrm{T}} P_k \tilde{x}_k \leq \varepsilon\}$
6: **ONLINE**
7: Initialize at $k = 0$
8: **while** $k < T_{\text{final}}$
9: **if** $\tilde{x}_k \in \mathbb{W}_k$ **then**
10: Set $\tilde{u}_k = K_k \tilde{x}_k$
11: **else**
12: Utilize an SQP procedure [28] to produce a feasible virtual control sequence $\tilde{\boldsymbol{u}}_k^*$.
13: Apply $\tilde{u}_k = \tilde{u}_{k|k}^*$
14: **end if**
15: Apply $u_k = u_k^r + \tilde{u}_k$
16: $k \leftarrow k + 1$
17: **end while**

Let us note that the linear control law can be appended as the control input at the end of the horizon to accelerate the convergence of the numerical procedure, i.e., to serve as a "warm start" $\tilde{\boldsymbol{u}}_k = \{\tilde{u}_{k|k-1}, \tilde{u}_{k+1|k-1}, \ldots, \tilde{u}_{k+N-2|k-1}, K_{k+N-1} \tilde{x}_{k+N-1}\}$.

The following theorem completes the stability analysis for the closed-loop system controlled by the DMMPLC described in Algorithm 1.

THEOREM 1. (Stability of the dual-mode tracking control).

Let $\mathbb{W}_k$ *be defined per Proposition 1. The DMMPLC described by Algorithm 1 renders the point* $\tilde{x} = 0$, *and hence, the reference trajectory* $\underline{\boldsymbol{x}}^r$, *stable for the entire control task* $k \in \{0, 1, \ldots, T_{\text{final}}\}$.

Proof. The proof of the overall stability is established by showing that sufficient cost reduction can be ensured for a control sequence that contains an MPC determined sequence with a linear control term appended at the end. □

4 Control of an HVAC Central Air Handling Unit

A simulated implementation of the proposed dual-mode control strategy to the central AHU of a two-zone VAV HVAC system is

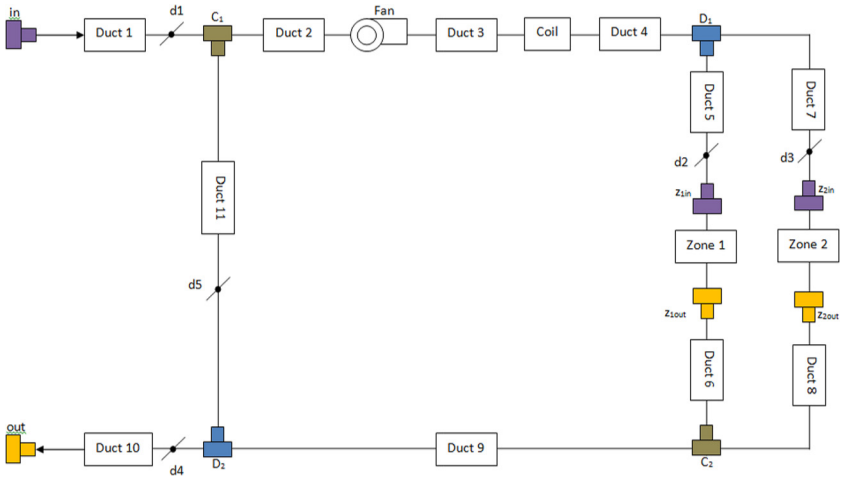

Fig. 1 Schematic of the AHU system

Table 1 Equations and descriptions of terms involved in the state-space equations of the AHU system

Term	Formula
Pressure drop across damper i	$\Delta P_{d_i} = \dfrac{\dot{m}_i \exp\left(a + b\left[(1-u_{d_i})\theta_{\max}\right]^c\right)}{2\rho A_{\text{vav}}^2}$
Pressure drop across the fan	$\Delta P_F = ch\rho\left[DN_f\left(displaystyle\frac{n_m}{n_f}\right)\right]^2$
Pressure drop across converging T-junction i (straight exit)	$\Delta C_i = \dfrac{\left[(1+\xi)\left(\dot{m}_i^{\text{in}}\right)^2 - \left(\dot{m}_i^{\text{out}}\right)^2\right]}{2\rho A_i^2}$
Pressure drop across converging T-junction i (elbowed exit)	$\Delta C_{iT} = \dfrac{\left[(1+\xi_T)\left(\dot{m}_i^{\text{in}}\right)^2 - \left(\dot{m}_i^{\text{out}}\right)^2\right]}{2\rho A_i^2}$
Pressure drop across diverging T-junction i (straight exit)	$\Delta D_i = \dfrac{\left[(1-\xi)\left(\dot{m}_i^{\text{in}}\right)^2 - \left(\dot{m}_i^{\text{out}}\right)^2\right]}{2\rho A_i^2}$
Pressure drop across diverging T-junction i (elbowed exit)	$\Delta D_{iT} = \dfrac{\left[(1-\xi_T)\left(\dot{m}_i^{\text{in}}\right)^2 - \left(\dot{m}_i^{\text{out}}\right)^2\right]}{2\rho A_i^2}$
Pressure drop across entry junction i	$\Delta P_i^{\text{in}} = \dfrac{\xi_i^{\text{in}}\dot{m}_i^2}{2\rho A_i^2}$
Pressure drop across exit junction i	$\Delta P_i^{\text{out}} = \dfrac{\xi_i^{\text{out}}\dot{m}_i^2}{2\rho A_i^2}$
Pressure drop due to friction in duct i	$f_i = \dfrac{A_d c_f L_i \dot{m}_i^2}{2\rho A_i^3}$

$\dot{m}_i$ is the air mass flow rate through component i; A_{vav} is the cross-sectional area of the terminal boxes (dampers); a, b, and c are the damper parameters; ch is the dimensionless pressure head coefficient; D is the fan impeller diameter; n_m/n_f is the motor and fan speed ratio; ξ, ξ_T, ξ_i^{in}, and ξ_i^{out} are the junction friction coefficients; A_i is the cross-sectional area of component i; A_d is the duct perimeter; c_f is the duct surface friction coefficient; L_i is the length of duct i; and ρ is the air density.

presented in this section. Typically, HVAC systems related applications of MPC have been in the supervisory control role [31]. However, the airflow subsystem considered here offers different challenges due to the significantly faster dynamics than the system thermodynamics, which are the subject of supervisory control tasks.

4.1 Air Handling Unit System Model. The AHU system considered is comprised of a fan, five dampers, ductwork, multiple T-junctions, and entry and exit junctions. A schematic of the system is provided in Fig. 1, and the system dynamics are developed along the lines described in Ref. [32], with specific component models developed following Refs. [33,34].

The AHU system dynamics are developed using five states and six inputs

Table 2 AHU system and component parameters utilized for the simulations presented in this work

Fan		Air		T-junctions	
ch	1.41	μ_a (N s/m^2)	184.6×10^{-7}	ξ	0.9
b	0.01	ρ (kg/m^3)	1.1614	ξ_T	2
κ	10	Zones		Dampers	
k_i	1.867	V_{z_1} (m^3)	280	a	–0.06
k_b	1.867	V_{z_2} (m^3)	280	b	2.52
R	0.5	Ducts		c	3.35
L	1	A_i(m^2)	0.25	A_{vav} (m^2)	0.25
η	0.9	A_d (m)	2	$\theta_{\max}$ (rad)	1.2
$\frac{n_m}{n_f}$	3.7	L_i (m)	25		

Table 3 Performance indicators for comparison of the proportional–integral–differential (PID) control and DMMPLC, as simulated with the AHU system

	Unfiltered step shift		Filtered step shift		Trajectory tracking	
Performance indicators	PID	DMMPLC	PID	DMMPLC	PID	DMMPLC
Power consumption (W)	956.8	798.0	953.7	527.5	1054.3	598.3
Zone 1 airflow final error 1	$O(10^{-1})$	$O(10^{-8})$	$O(10^{-2})$	$O(10^{-8})$	N/A	N/A
Zone 1 airflow final error 2	$O(10^{-4})$	$O(10^{-7})$	$O(10^{-4})$	$O(10^{-7})$	N/A	N/A
Zone 2 airflow final error 1	$O(10^{-3})$	$O(10^{-8})$	$O(10^{-3})$	$O(10^{-8})$	N/A	N/A
Zone 2 airflow final error 2	$O(10^{-3})$	$O(10^{-5})$	$O(10^{-3})$	$O(10^{-8})$	N/A	N/A
Fresh airflow final error 1	$O(10^{-6})$	$O(10^{-8})$	$O(10^{-6})$	$O(10^{-8})$	N/A	N/A
Fresh airflow final error 2	$O(10^{-5})$	$O(10^{-5})$	$O(10^{-8})$	$O(10^{-8})$	N/A	N/A
Zone 1 airflow settling time 1	>20	4	>20	3	N/A	N/A
Zone 1 airflow settling time 2	16	4	0	0	N/A	N/A
Zone 2 airflow settling time 1	12	4	12	4	N/A	N/A
Zone 2 airflow settling time 2	8	4	0	0	N/A	N/A
Fresh airflow settling time 1	18	4	18	1	N/A	N/A
Fresh airflow settling time 2	13	4	>20	0	N/A	N/A

Settling times are rounded to the nearest second, and final errors are expressed in order to magnitude.

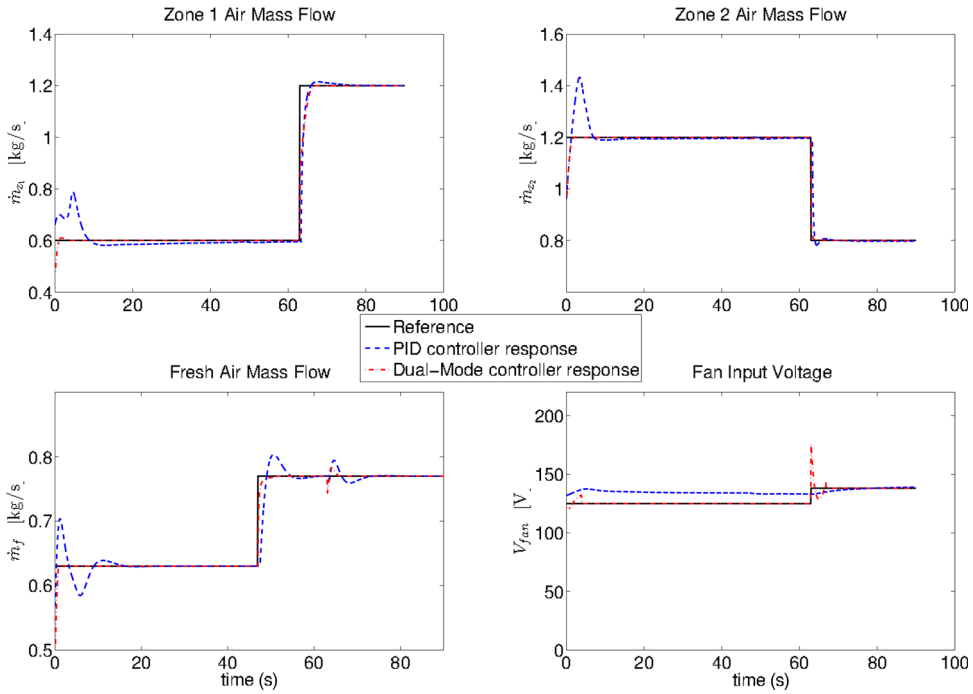

Fig. 2 Results of simulated tracking of a step shift with DMMPLC and PID control. The results include all the output references and achieved trajectories, as well as the fan supply voltage.

$$x^{\mathrm{T}} = [\dot{m}_f, \dot{m}_s, \dot{m}_{z_1}, N_F, I_F]$$
$$u^{\mathrm{T}} = [u_F, u_{d_1}, u_{d_2}, u_{d_3}, u_{d_4}, u_{d_5}]$$

where $\dot{m}_f$ is the fresh air mass flow rate (kg/s), $\dot{m}_s$ is the supply air mass flow (kg/s), $\dot{m}_{z_1}$ is the air mass flow to zone 1 (kg/s), N_F is the fan-motor speed (rev/s), I_f is the fan-motor current (A), u_F is the fan supply voltage, and $u_{d_n}, n = 1, 2, ..., 5$ is the position of damper $n \in [0, 1]$. For the dampers, zero signifies a fully closed damper and one the fully open case. The simplest expression of the dynamics is made by developing the expression associated with the air flow rates separately from the equations for the fan states. Following Ref. [32], the dynamics of the fan are given by

$$\dot{N}_F = \frac{1}{\kappa}\left(\frac{k_i I_F}{2\pi} - bN_F - \frac{\Delta P_F \dot{m}_s}{(2\pi)^2 \eta N_F}\right) \tag{9}$$

$$\dot{I}_F = \frac{1}{L}(u_F - RI_F - 2\pi k_b N_F) \tag{10}$$

where κ is the fan-motor equivalent moment of inertia (kg/m^2), k_i is the fan torque constant (N · m rev/A), b is the fan friction factor (kg/m^2/s), ΔP_F is the pressure change across fan (N/m^2), η is the fan efficiency, L is the fan armature inductance (H), R is the fan supply resistance (Ω), and k_b is the back electromotive force constant (V s/rad). Equations (9) and (10) yield two of the five state equations for the system model, while the remaining three pertain to the dynamics of the air flows and are described as follows [32]:

$$\begin{bmatrix} \ddot{m}_f \\ \ddot{m}_s \\ \ddot{m}_{z_1} \end{bmatrix} = \mathcal{L}^{-1} \begin{bmatrix} g_1(x,u) \\ g_2(x,u) \\ g_3(x,u) \end{bmatrix} \tag{11}$$

where g_1, g_2, and g_3 are the sum of all the pressure changes in the fresh air loop, supply air loop, and zone loop, respectively (i.e., the three separable closed-loops from left to right in Fig. 1), while $\mathcal{L}$ is a matrix of constants dependent on the system component dimensions. For instance,

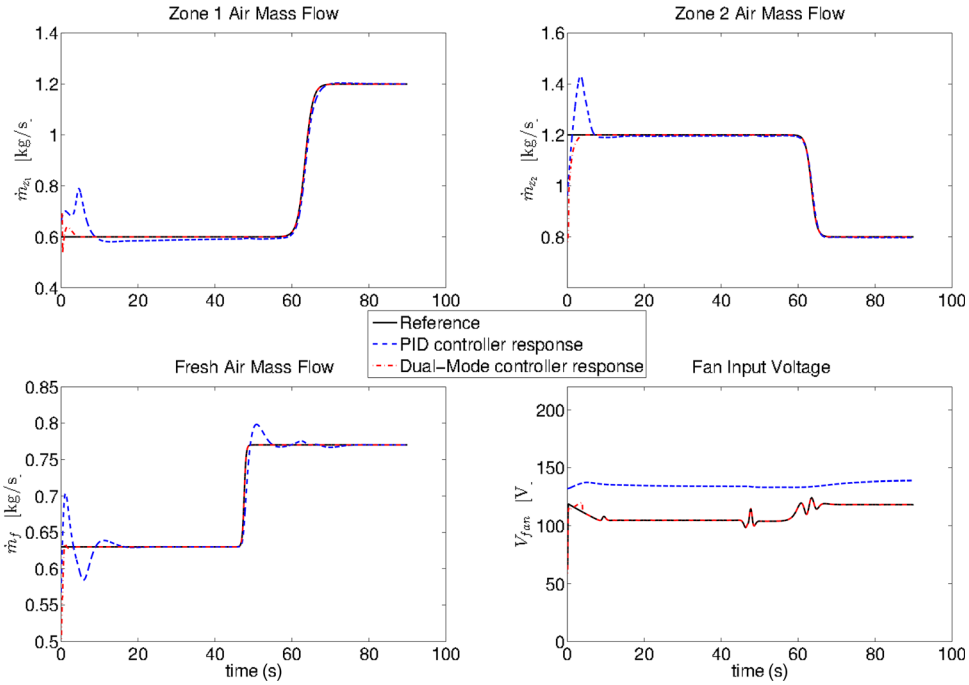

Fig. 3 Results of simulated tracking of a filtered step shift with DMMPLC and PID control. The results include all the output references and achieved trajectories, as well as the fan supply voltage.

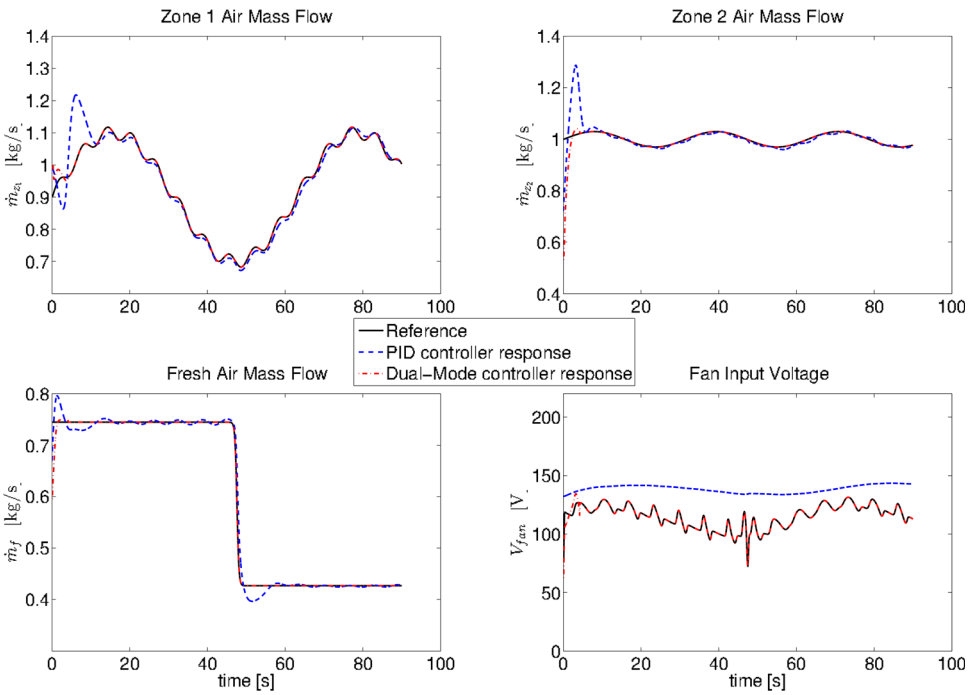

Fig. 4 Results of simulated tracking of a generic trajectory with DMMPLC and PID control. The results include all the output references and achieved trajectories, as well as the fan supply voltage.

$$g_1 = \Delta P_{d_1} - \Delta P_{d_4} + \Delta P_{d_5} - \Delta C_1 + \Delta C_{1T} + \Delta D_2 - \Delta D_{2T} + \Delta P_{\text{out}} - \Delta P_{\text{in}} - f_1 - f_{10} + f_{11}$$

with each term in the above expressions representing a pressure change across a component in the concerned air flow loop, and the component description as well as equations for each of these are provided in Table 1. The expressions for g_2 and g_3 can be obtained in the same manner.

The matrix $\mathcal{L}$, on the other hand, is given by

$$\mathcal{L} = \begin{bmatrix} \frac{L_1}{A_1} + \frac{L_{10}}{A_{10}} + \frac{L_{11}}{A_{11}} & -\frac{L_{11}}{A_{11}} & 0 \\ -\frac{L_{11}}{A_{11}} & -\frac{L_2}{A_2} + \frac{L_3}{A_3} + \frac{L_9}{A_9} + -\frac{L_{11}}{A_{11}} & \frac{L_5}{A_5} + \frac{L_6}{A_6} \\ 0 & -\frac{L_7}{A_7} - \frac{L_8}{A_8} & \frac{L_5}{A_5} + \frac{L_6}{A_6} + \frac{L_7}{A_7} + \frac{L_8}{A_8} \end{bmatrix}$$

where L_i and A_i are the length and cross-sectional area of duct i, respectively. For simplicity and without loss of generality, all the ducts are assumed to have identical dimensions in the case presented here. The system parameters used have been summarized in Table 2 and are based on the information given in Refs. [33–35].

The system outputs are obtained from the states as $y = Cx$, where $C = \text{diag}([1, 1, 1, 0, 0])$. Hence, this is a nonlinear multi-input multi-output dynamic system with five states, three outputs, and six inputs. It should also be pointed out that, in general, only two output references can be freely assigned, as the fresh air flow is constrained to meet ASHRAE standards [36]. The system dynamics are discretized using a sampling rate of 10 Hz and the forward Euler method [37].

4.2 Simulation Results. In this section, the performance of the proposed controller is presented in comparison with a PID control structure. The PID controllers prescribe the control inputs to the building entry damper, the two-zone entry dampers, and the fan, while the recirculation and exhaust dampers remain fully open at all times. The damper inputs are assigned so as to maintain the desired air flows through the system, whereas the fan supply voltage maintains the static-pressure two-thirds of the length down the ducts to the serviced zones. Such fan control logic is commonly used in VAV HVAC implementations[3] [38]. It is known that higher set-points for the static pressure lead to greater control authority, but also result in greater energy consumption. The set-points used in the current simulations were set so as to allow all the desired levels of flow to be achievable, although no attempt was made to optimize them.

In the simulations, the MPC horizon is 4 s, the total time is $T_{\text{final}} = 90$ s, and numerical performance indicators are presented in Table 3. Details about the determination of $\boldsymbol{u}^r$ and $\boldsymbol{x}^r$ via the auxiliary problem are provided in the Appendix.

4.2.1 Step Shift. Since the control goal is to quickly achieve the set points with minimal energy consumption, three main performance indicators are considered: the settling time to a given reference level, the errors after a given time into a task, and the energy consumption.

In the case presented here, the reference trajectory incorporates a single step shift from $r_{\text{initial}} = [0.63\ 0.90\ 1.00]^{\text{T}}\text{kg/s}$ to $r_{\text{final}} = [0.77\ 1.20\ 0.80]^{\text{T}}\text{kg/s}$, with the transitions occurring at different times. The dual-mode controller is informed only of the current reference level, hence the control algorithm must be reinitialized at the moment of shift in any output reference level. The simulated results are presented in Fig. 2.

The DMMPLC forces the full system state into the region, where the linear controller can be implemented within the 4 s horizon. Hence, the MPC algorithm is only employed for 8 s. The DMMPLC performance is fairly consistent, while the PID controller performance is clearly quite sensitive to the transitions demanded. Additionally, the supply voltage demanded by the fan is greater under the PID controller.

4.2.2 Filtered Step Shift. A common technique to ensure smoothness of trajectories in control applications is to filter discontinuous trajectories [39,40]. In this example, the reference trajectory was filtered using a finite impulse response filter, and the tracking results are presented in Fig. 3. From these results, it is obvious that the dual-mode controller leads to a shorter settling time for all the outputs and that the required supply voltage to the fan is also visibly lower.

[3]It is worth pointing out that there have been advances in this control approach, which allow for reduced energy consumption through the use of static-pressure set-point reset logic.

4.2.3 Trajectory Tracking. In order to evaluate the trajectory tracking capabilities of the DMMPLC, time-varying reference trajectories are assigned as follows:

$$\dot{m}_{z_1} = 0.9 + 0.2\sin(0.1t) - 0.02\sin(t)$$
$$\dot{m}_{z_2} = 1.0 + 0.03\sin(0.2t)$$
$$\dot{m}_f = \begin{cases} 0.63, & \text{if } t \le 47.5\text{ s} \\ 0.77, & \text{otherwise} \end{cases}$$

The results for the simulations under both controllers are presented in Fig. 4.

While the dual-mode controller is once again able to drive the system to the reference trajectory and continue tracking it for the entire simulated time period, the PID controller is unable to accurately track any of the desired output trajectories. While HVAC applications do not usually require such time-varying trajectory tracking, the ability to track more general trajectories would allow greater flexibility for the HVAC supervisory controller, which may in turn lead to reductions in energy consumption.

To summarize, the contents of Table 3 clearly show that the newly introduced controller is preferable to the PID control structure in terms of the listed performance measures. Most notably, the average power consumption is significantly lower for the dual-mode controller. Additionally, the final error, measured as the tracking error at the 25 s mark after a reference level is set, is always smaller with the dual-mode controller than that under the PID control structure.

5 Conclusions and Future Work

The DMMPLC algorithm proposed in this paper enables trajectory tracking for discrete-time nonlinear dynamic systems, by utilizing a nonpoint terminal constraint set as the switching surface between the MPC and linear controllers. The proposed approach extends the dual-mode control concept, which guarantees closed-loop stability in a practical manner by overcoming the need to find the globally optimal solution or satisfy a terminal equality constraint in the MPC implementation. This allows for termination of the optimization procedure underlying the MPC in a finite number of iterations. Formal characterization of the switching surface and the associated proof of stability have been provided in this document. Furthermore, the newly proposed control scheme was applied to simulate control of the central AHU of a two-zone VAV HVAC system, and it was shown to provide performance improvement over a commonly used PID control structure.

There are several natural extensions of this work. First, it is necessary to expand the control algorithm presented here by considering various factors that would enable it to deal with common uncertainty sources, e.g., imperfectly known disturbances and model. Beyond these extensions, other applications of the DMMPLC presented in this paper can also be considered. For example, control of the entire HVAC system would introduce challenges in handling systems with different rates of dynamic behavior, as well as different sampling rates.

Appendix: Auxiliary Optimization for $\underline{\boldsymbol{x}}^r$ and $\underline{\boldsymbol{u}}^r$

Given a reference trajectory $\underline{\boldsymbol{r}}$ and Assumption 3, a control sequence $\underline{\boldsymbol{u}}^r$ that leads to perfect tracking can be determined by solving an auxiliary optimal control problem. As was mentioned in Sec. 2, the output may not be dependent on all the states of the system, which may lead to multiple potential reference control sequences. This yields another degree-of-freedom in satisfying the tracking objective, which can be addressed as below

$$\underset{\underline{\boldsymbol{x}}^r, \underline{\boldsymbol{u}}^r}{\text{minimize}} \quad J^{\text{aux}}(\underline{\boldsymbol{x}}^r, \underline{\boldsymbol{u}}^r) = \sum_{i=0}^{T_{\text{final}}-1} (l^{\text{aux}}(x_i^r, u_i^r)) + V_f^{\text{aux}}(x_{T_{\text{final}}}^r)$$
$$\text{subject to:} \quad x_{k+1}^r = f(k, x_k^r, u_k^r), \text{ for } k = 0, 1, \ldots, T_{\text{final}} - 1$$
$$h(x_k^r) = r_k$$

where $l^{\text{aux}}(x_i^r, u_i^r) = x_i^{r^{\mathrm{T}}} Q^{\text{aux}} x_i^r + u_i^{r^{\mathrm{T}}} R^{\text{aux}} u_i^r$ and $V_f^{\text{aux}}(x_{T_{\text{final}}}^r) = x_{T_{\text{final}}}^{r^{\mathrm{T}}} Q_f^{\text{aux}} x_{T_{\text{final}}}^r$. The matrices Q^{aux}, R^{aux}, and Q_f^{aux} are symmetric and positive semidefinite.

In the HVAC AHU control application, the reference inputs $\underline{\boldsymbol{u}}^r$ are determined so as to minimize energy consumption and avoid completely opening or closing the dampers to maintain control authority. Additionally, a penalty is employed for high rates of changes in the reference control input. The numerical values of the matrices used were $Q_f^{\text{aux}} = Q^{\text{aux}} = \text{diag}([1, 1, 1, 0, 0])$ and $R^{\text{aux}} = ([2, 1, 1, 1, 1, 1])$.

References

[1] Morari, M., and Lee, J. H., 1999, "Model Predictive Control: Past, Present and Future," Comput. Chem. Eng., **23**(4–5), pp. 667–682.

[2] Diehl, M., Findeisen, R., Schwarzkopf, S., Uslu, I., Allgöwer, F., Bock, H. G., Gilles, E. D., and Schlöder, J. P., 2003, "An Efficient Algorithm for Nonlinear Model Predictive Control of Large-Scale Systems—Part II: Experimental Evaluation for a Distillation Column," Automatisierungstechnik, **51**(1), pp. 22–29.

[3] Camacho, E. F., and Bordons, C., 1999, *Model Predictive Control*, Springer, New York.

[4] Qin, S. J., and Badgwell, T. A., 2003, "A Survey of Industrial Model Predictive Control Technology," Control Eng. Pract., **11**(7), pp. 733–764.

[5] Rawlings, J. B., and Mayne, D. Q., 2000, *Model Predictive Control: Theory and Design*, Nob Hill Publishers, Madison, WI.

[6] Grune, L., and Pannek, J., 2011, *Nonlinear Model Predictive Control: Theory and Algorithms*, Springer-Verlag, London.

[7] Ahmad, Z., and Zhang, J., 2006, "A Nonlinear Model Predictive Control Strategy Using Multiple Neural Networks Models," Adv. Neural Networks, **3972**, pp. 943–948.

[8] Dziekan, L., Witczak, M., and Korbicz, J., 2011, "A Predictive Fault-Tolerant Control Scheme for Takagi–Sugeno Fuzzy Systems," IFAC Proc. **44**(1), pp. 4684–4689.

[9] Mu, J., and Rees, D., 2004, "Approximate Model Predictive Control for Gas Turbine Engines," 2004 American Control Conference, June 30–July 2, pp. 5704–5709.

[10] Michalska, H., and Mayne, D. Q., 1993, "Robust Receding Horizon Control of Constrained Nonlinear Systems," IEEE Trans. Autom. Control, **38**(1), pp. 1623–1633.

[11] Chen, H., and Allgöwer, F., 1998, "A Quasi-Infinite Horizon Nonlinear Model Predictive Control Scheme With Guaranteed Stability," Automatica, **34**(10), pp. 1205–1217.

[12] Scokaert, P. O. M., Mayne, D. Q., and Rawlings, J. B., 1999, "Suboptimal Model Predictive Control (Feasibility Implies Stability)," IEEE Trans. Autom. Control, **44**(3), pp. 648–654.

[13] Nguyen, H., and Gutman, P., 2013, "A New Dual-Mode Model Predictive Control for Constrained Linear Systems," 21st Mediterranean Conference on Control and Automation (MED), Vol. 4, pp. 1393–1397.

[14] Al-Gherwi, W., Budman, H., and Elkamel, A., 2013, "A Robust Distributed Model Predictive Control Based on a Dual-Mode Approach," Comput. Chem. Eng., **50**(1), pp. 130–138.

[15] Acikmese, A. B., and Carson, J. M., III, 2006, "A Nonlinear Model Predictive Control Algorithm With Proven Robustness and Resolvability," 2006 American Control Conference, June 14–16, pp. 887–893.

[16] Stephens, M. A., Manzie, C., and Good, M. C., 2013, "Model Predictive Control for Reference Tracking on an Industrial Machine Tool Servo Drive," IEEE Trans. Ind. Inf., **9**(2), pp. 808–816.

[17] Simon, D., Löfberg, J., and Glad, T., 2014, "Reference Tracking MPC Using Dynamic Terminal Set Transformation," IEEE Trans. Autom. Control, **59**(10), pp. 2790–2795.

[18] Limon, D., Alamo, T., de la Pena, D. M., Zeilinger, M., Jones, C., and Periera, M., 2012, "MPC for Tracking Periodic Reference Signals," IFAC Proc. Vol., **45**(17), pp. 490–495.

[19] Chisci, L., Falugi, P., and Zappa, G., 2005, "Predictive Tracking Control of Constrained Nonlinear Systems," IEEE Proc. Control Theory Appl., **152**(3), pp. 309–316.

[20] Magni, L., Nicolao, G. D., Magnani, L., and Scattolini, R., 2001, "A Stabilizing Model-Based Predictive Control Algorithm for Nonlinear Systems," Automatica, **37**(9), pp. 1351–1362.

[21] Kuhne, F., Gomes, J. M., and Lages, W. F., 2005, "Mobile Robot Trajectory Tracking Using Model Predictive Control," VII SBAI/II IEEE LARS, pp. 1–7.

[22] Faulwasser, T., and Findeisen, R., 2011, "A Model Predictive Control Approach to Trajectory Tracking Problems Via Time-Varying Level Sets of Lyapunov Functions," 50th IEEE Conference on Decision and Control and European Control Conference (CDC-ECC), Dec. 12–15, pp. 3381–3386.

[23] Kazantzis, N., Chong, K. T., Park, J. H., and Parlos, A. G., 2005, "Control-Relevant Discretization of Nonlinear Systems With Time-Delay Using Taylor-Lie Series," ASME J. Dyn. Syst. Meas. Control, **127**(1), p. 153.

[24] Vaclavek, P., and Blaha, P., 2013, "PMSM Model Discretization for Model Predictive Control Algorithms," 2013 IEEE/SICE International Symposium on System Integration, Dec. 15–17, Vol. 3, pp. 13–18.

[25] Sakamoto, T., Noriyuki, H., and Ochi, Y., 2011, "Exact Linearization and Discretization of Nonlinear Systems Satisfying a Lagrange PDE Condition," Trans. Can. Soc. Mech. Eng., **35**(2), pp. 215–228.

[26] Mayne, D. Q., Rawlings, J. B., Rao, C. V., and Scokaert, P. O. M., 2000, "Constrained Model Predictive Control: Stability and Optimality," Automatica, **36**(6), pp. 789–814.

[27] Keerthi, S. S., and Gilbert, E. G., 1988, "Optimal Infinite-Horizon Feedback Laws for a General Class of Constrained Discrete-Time Systems: Stability and Moving-Horizon Approximations," J. Optim. Theory Appl., **57**(2), pp. 265–293.

[28] Rodriguez, L. A., and Sideris, A., 2011, "A Sequential Linear Quadratic Approach for Constrained Nonlinear Optimal Control," American Control Conference (ACC), pp. 1470–1475.

[29] Khalil, H. K., 1996, *Nonlinear Systems*, 2nd ed., Prentice Hall, Upper Saddle River, NJ.

[30] Lagarias, J. C., Reeds, J. A., Wright, M. H., and Wright, P. E., 1998, "Convergence Properties of the Nelder-Mead Simplex Method in Low Dimensions," SIAM J. Optim., **9**(1), pp. 112–147.

[31] Kwadzogah, R., Zhou, M., and Li, S., 2013, "Model Predictive Control for HVAC Systems—A Review," 2013 IEEE International Conference on Automation Science and Engineering (CASE), Aug. 17–20, pp. 442–447.

[32] Zaheer-Uddin, M., and Zheng, G., 1994, "A VAV System Model for Simulation of Energy Management Control Functions: Off Normal Operation and Duty Cycling," Energy Convers. Manage., **35**(II), pp. 917–931.

[33] Underwood, C., and Yik, F. W. H., 2004, *Modelling Methods for Energy in Buildings*, Blackwell Science, Oxford, UK.

[34] McQuinston, F., Parker, J., and Spitler, J., 2005, *Heating, Ventilation and Air Conditioning—Analysis and Design*, Wiley, Hoboken, NJ.

[35] Incropera, F. P., and DeWitt, D. P., 2001, *Introduction to Heat Transfer*, 4th ed., Wiley, New York.

[36] ASHRAE, 2004, "Ventilation for Acceptable Indoor Air Quality," American Society of Heating, Refrigerating, and Air-Conditioning Engineers, Inc.: Atlanta, GA Standard No. ANSI/ASHRAE Standard 62-2001.

[37] Butcher, J. C., 2003, *Numerical Methods for Ordinary Differential Equations*, Wiley, West Sussex, UK.

[38] Murphy, J., 2011, "High-Performance VAV Systems," ASHRAE J., **53**(10), pp. 18–28.

[39] Zanasi, R., Guarino Lo Bianco, C., and Tonielli, A., 2000, "Nonlinear Filters for the Generation of Smooth Trajectories," Automatica, **36**(3), pp. 439–448.

[40] Bonfè, M., and Secchi, C., 2010, "Online Smooth Trajectory Planning for Mobile Robots by Means of Nonlinear Filters," IEEE/RSJ 2010 International Conference on Intelligent Robots and Systems (IROS 2010), Oct. 18–22, pp. 4299–4304.